Study on mechanical properties and microstructure of steel-polypropylene fiber coal gangue concrete

Jiuyang Li, Li Chen*, Jingwei Luo, Yuepeng Zhu, Xinmei Fan and Guangchao Hu

School of Civil Engineering, Changchun Institute of Technology, Changchun, China

Incorporating coal gangue into the concrete matrix can realize the utilization of solid waste and reduce the use of natural aggregate. To improve the mechanical properties of coal gangue concrete, this paper designs four-level and four-factor orthogonal tests with coal gangue ceramide substitution rate, coal gangue ceramide sand substitution rate, steel fiber content, and polypropylene fiber content as independent variables. Through multidimensional data analysis of the test results, The main and secondary factors of compressive strength of hybrid fiber coal gangue concrete from strong to weak are the replacement rate of coal gangue ceramic sand, the replacement rate of coal gangue ceramic grain, the content of steel fiber and the content of polypropylene fiber. The optimal content is 30% coal gangue ceramic particle, 25~30% coal gangue ceramic sand, 0.75~1% steel fiber, and 0.2% polypropylene fiber. The grey prediction model GM (1, 5) is obtained, which can predict the concrete strength well within the range selected in this paper. The influence of fiber and coal gangue on the microstructure was studied by scanning electron microscopy, and the influence law of interfacial transition zone on the strength of concrete was explored, which provided a theoretical basis for the study of solid waste utilization of coal gangue.

KEYWORDS

steel fiber, polypropylene fiber, coal gangue, compressive strength, micro properties, grey prediction model

1 Introduction

Coal gangue is an associated organism produced in the coal mining process, and its large accumulation will harm the natural environment (Huang et al., 2018; Li et al., 2023a; Zhang et al., 2023a). The application of coal gangue in concrete as a building material is in line with the concept of green environmental protection. Therefore, many scholars have carried out studies on coal gangue concrete, proving that coal gangue can be added to concrete instead of natural aggregate, and the strength of concrete decreases with the increase of coal gangue content (Huang, 2015; Yan, 2017a). Zhou M (ZHOU et al., 2011; Zhou et al., 2013; Zhou et al., 2019; Li et al., 2022a) conducted a detailed study on the physical and chemical properties and mechanical properties of raw aggregate from coal gangue, prepared C30 concrete with coal gangue, and studied its failure mode and microscopic morphology. Yu L (Yu et al., 2022) studied the macro and
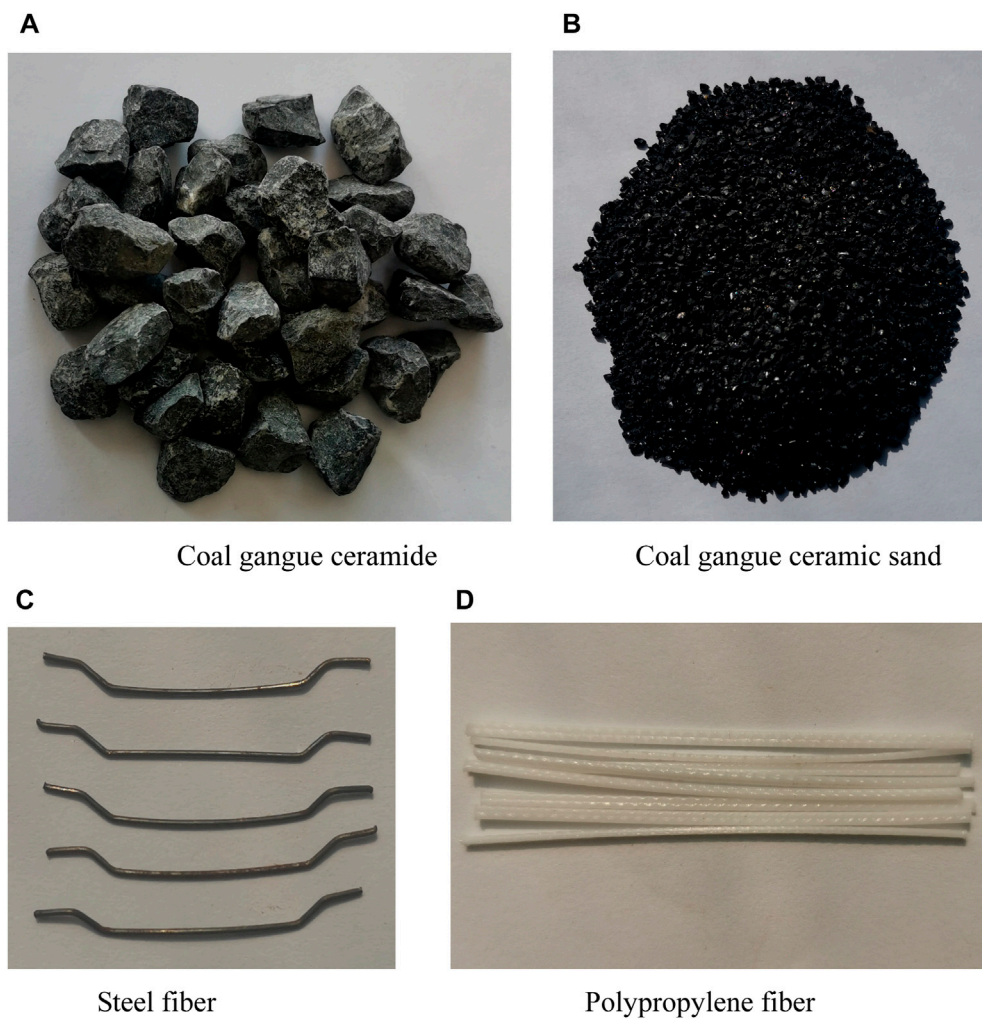
FIGURE 1
Raw materials. **(A)** Coal gangue ceramide **(B)** Coal gangue ceramic sand **(C)** Steel fiber **(D)** Polypropylene fiber.

micro properties of coal gangue concrete and mortar and concluded that the performance was optimal when the coal gangue content was 25%.

To make better use of coal gangue in concrete, it is necessary to add some materials into concrete to improve its performance. Fiber is widely used in construction, transportation, water conservancy, and other engineering fields due to its advantages of toughening and good crack resistance (Liu et al., 2022; Qiu et al., 2022). At present, the research of scholars has shifted from single-fiber concrete to hybrid-fiber concrete. Hybrid fiber concrete produces functional complementarity of different kinds of fibers in concrete, resulting in a hybrid effect of 1 + 1 > 2 (Guan et al., 2023). However, steel-polypropylene hybrid fiber is one of the most studied types at present (Afroughsabet and Ozbakkaloglu, 2015; Xu et al., 2016; Zhang et al., 2022a). Relevant studies have shown (Li et al., 2022b; Zhang et al., 2022b; Feng et al., 2022) that steel fiber with high elastic modulus can improve the ultimate strength of concrete, while polypropylene fiber with low elastic modulus and high

TABLE 1 Composition of coal gangue.

Composition	SiO_2	Al_2O_3	Fe_2O_3	Other
Content (%)	56.49	30.43	7.82	5.26

ductility can improve the toughness and post-crack strain capacity of concrete.

Based on this, this paper adopts a four-level orthogonal test method with four factors (substitution rate of coal gangue ceramide for coarse aggregate, substitution rate of coal gangue ceramide for fine aggregate, steel fiber content, and polypropylene fiber content) to study the compressive strength and splitting tensile strength of concrete cube. Using range analysis, variance analysis, and grey correlation theory, the paper also adopts the orthogonal test method. The influence of different factors on the compressive strength and splitting tensile strength of concrete was analyzed, and then the strength prediction model of GM (1, 5) steel-polypropylene fiber coal gangue concrete was established. In addition, the

TABLE 2 Material parameter.

Coal gangue	Apparent density	Bulk density	24 h water absorption
	2791 kg/m³	1287 kg/m³	6.35%
Steel fiber	Length	Length-diameter ratio	Tensile strength
	25 mm	50	1,000~1,800 MPa
Polypropylene fiber	Length	Density	Tensile strength
	50 mm	0.91 g/cm³	720 MPa

TABLE 3 Concrete mix design.

Composition	Water	Cement	Sand	Stone
Content (kg/m³)	220	366.67	725.33	1087.99

TABLE 4 Experimental factors and levels.

Level	Factor			
	A (%)	B (%)	C (%)	D (%)
1	25	25	0.25	0.1
2	30	30	0.50	0.2
3	35	35	0.75	0.3
4	40	40	1.00	0.4

failure mechanism of steel-polypropylene fiber coal gangue concrete (SF-PF CGrc) was analyzed from the microscopic level. To provide a theoretical basis for the strength prediction of coal gangue concrete and its application in engineering.

2 Overview of the experiment

2.1 Materials

Cement is Dinglu brand ordinary Portland cement. Coarse aggregate is ordinary gravel with a particle size range of 5~16 mm. Fine aggregate is natural river sand with a fineness modulus of 2.61 and a particle size range of 0.075~4.750 mm. The coal gangue is the secondary processed ceramide and sand provided by Chaoyang Hualong Co., LTD., as shown in Figures 1A, B, and its composition is shown in Table 1. End-hook steel fiber and polypropylene fiber are used, as shown in Figures 1C, D, and the performance parameters of the above materials are shown in Table 2. The water is ordinary tap water.

2.2 Design of mix proportion

According to "Ordinary concrete mix Design Regulations" (JGJ 55-2011) (China Academy of Building Research, 2011) and "Steel Fiber Concrete" (JG/T 472-2015) (Institute of Standard Quotas and Ministry of Housing and Urban-Rural Development, 2015), the C30 concrete mix of this test is calculated as shown in Table 3. Since this test involves the influence of multiple variables on mechanical property, the orthogonal test scheme of L16 (44) is designed in this paper to determine four factors, namely, the mass replacement rate of coal gangue ceramics (CGL, factor A), the mass replacement rate of coal gangue ceramics sand (CGS, factor B), the content of steel fiber (SF, factor C), and the content of polypropylene fiber (PF, factor D). Each factor corresponds to 4 levels. The test factors and levels are shown in Table 4. Ordinary concrete (PC) is set as the control group.

2.3 Specimen preparation and test method

Each test group was equipped with 6 cube test blocks of 100mm × 100mm × 100mm, 3 were used for cube compressive strength test and 3 were used for splitting tensile strength test. A total of 102 specimens were made. The test was carried out after 28 days of maintenance in the standard curing chamber. This test was conducted according to the Chinese specification GB/T 50081-2019 (Afroughsabet and Ozbakkaloglu, 2015). The loading equipment is an electro-hydraulic servo-hydraulic testing machine with a loading speed of 0.5 MPa/s and a maximum load accuracy of 0.01 Mpa. The cube compressive test is shown in Figure 2A and the axial compressive test is shown in Figure 2B.

Both cube compressive strength and axial compressive strength were obtained by dividing the maximum load value obtained from the test by the cross-sectional area of the specimen, multiplying it by a discount factor of 0.95, and analyzing the test results according to the test data processing method.

3 Analysis of orthogonal test results of steel-polypropylene fiber coal gangue concrete

The SF-PF CGrc specimen was tested, and the test results were shown in Table 5. The tensile and compression ratio (splitting tensile strength/cube compressive strength) is stable between 1/17 and 1/12, which is consistent with the tensile and compression ratio between 1/17 and 1/8 stipulated in the Principles of Concrete Structure Design (Liang et al., 2007), indicating that the test results are reliable, among which the cube compressive strength of group A1B2C2D2 is the highest, which is 24.62% higher than that of PC. The splitting
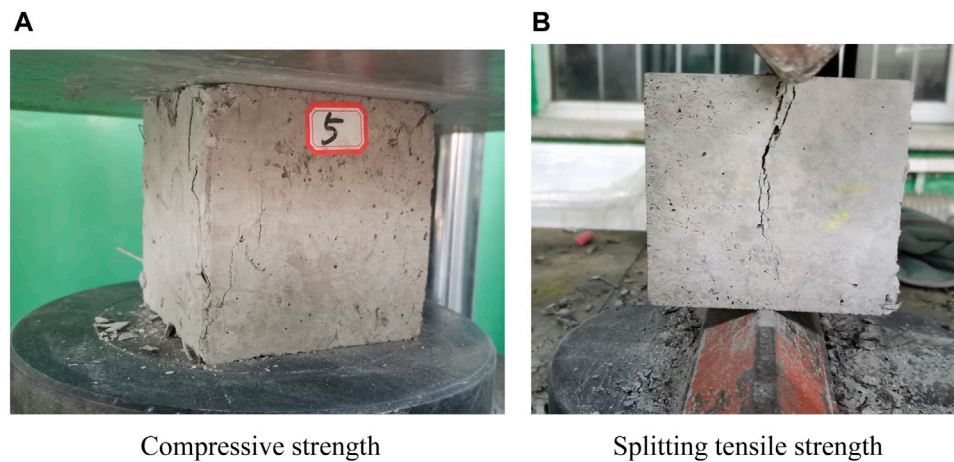
FIGURE 2
Test process diagram.

TABLE 5 SF-PF CGrc test results.

Group	Experiment number	Cube compressive strength/MPa	Splitting tensile strength/MPa	Tensile and compression ratio
1	A1B1C1D1	33.90	2.37	1/14.30
2	A1B2C2D2	37.20	2.65	1/14.04
3	A1B3C3D3	35.66	2.49	1/14.32
4	A1B4C4D4	34.50	2.36	1/14.62
5	A2B1C2D3	35.30	2.80	1/12.61
6	A2B2C1D4	36.28	2.48	1/14.63
7	A2B3C4D1	35.64	2.59	1/13.76
8	A2B4C3D2	34.97	2.34	1/14.94
9	A3B1C3D4	36.03	2.52	1/14.30
10	A3B2C4D3	35.84	2.46	1/14.81
11	A3B3C1D2	34.80	2.42	1/14.38
12	A3B4C2D1	32.63	1.95	1/14.30
13	A4B1C4D2	33.24	2.58	1/16.73
14	A4B2C3D1	35.98	2.46	1/14.63
15	A4B3C2D4	32.40	1.96	1/16.53
16	A4B4C1D3	32.50	1.96	1/14.58
17	PC	29.85	1.78	1/16.77

tensile strength of the A2B1C2D3 group was the highest, which was 57.3% higher than that of the PC group.

To explore the influence degree of different factors of coal gangue on the compressive strength and splitting tensile strength of concrete, range analysis, variance analysis, and grey correlation analysis were carried out on the test results to find out the significant influence degree of each factor, and GM (1,5) grey model was established to predict the strength.

3.1 Range analysis and variance analysis

Range analysis is simple and intuitive. The calculation amount is small, but the error cannot be estimated. The method introduced in reference (Li et al., 2023b) was used to analyze the experimental results. For range analysis, the greater the R, the greater the influence of the factor on the test results. According to the range analysis results in Table 6, the degree of influence of each factor on the concrete is as follows: B > A > C > D, that is, the replacement rate of

TABLE 6 Range analysis results.

Item	Cube compressive strength/MPa				Splitting tensile strength/MPa			
	Factor A	Factor B	Factor C	Factor D	Factor A	Factor B	Factor C	Factor D
Y_1	35.31	34.62	34.37	34.54	2.47	2.57	2.31	2.34
Y_2	35.55	36.33	34.38	35.05	2.55	2.51	2.34	2.50
Y_3	34.83	34.62	35.66	34.82	2.34	2.37	2.45	2.43
Y_4	33.53	33.65	34.80	34.80	2.24	2.15	2.50	2.33
R	2.02	2.67	1.29	0.51	0.31	0.42	0.19	0.17
Ranking of influencing factors	B > A > C > D							

Note: Y_i is the average intensity of each factor at the level of i.

TABLE 7 Variance analysis results.

Dependent variable	Factor	Deviation sum of squares	Degree of freedom	Mean square	F	Critical value	Significance
Cube compressive strength	A	12.18	3	4.06	5.08	$F_{0.05}(3, 3) = 9.28$ $F_{0.10}(3, 3) = 5.36$	(*)
	B	22.56	3	7.52	9.40		**
	C	4.39	3	1.46	1.83		—
	D	0.53	3	0.18	0.22		—
Splitting tensile strength	A	0.31	3	0.10	5.17		*
	B	0.41	3	0.14	6.88		(*)
	C	0.10	3	0.03	1.63		—
	D	0.07	3	0.02	1.23		—

Note:1)When $F > F_{0.0}(3,3)$ was an important significant factor, denoted **; 2) When $F_{0.10}(3, 3) < F < F_{0.05}(3,3)$, it is the general significant factor, denoted *; 3) When $F < F_{0.10}(3.3)$ but close to each other, it is a more significant factor, denoted as (*); 4) When $F < F_{0.10}(3,3)$ and the difference is large, it is not significant factor.

coal gangue ceramide sand > the replacement rate of coal gangue ceramide particle > steel fiber content > polypropylene fiber content.

To make up for the deficiency of range analysis, SPSS was used to further process the test results, and the results of variance analysis were obtained, as shown in Table 7. The significance level was selected, and $F_{0.05}(3, 3) = 9.28$ and $F_{0.10}(3, 3) = 5.36$ were obtained from the F distribution table. For the cube compressive strength, factor B was an important significant factor, while for the splitting tensile strength, factor B was a general significant factor. Considering the significance and F value of all factors, The order of influence degree of each factor on the experimental results is B > A > C > D, that is, the replacement rate of coal gangue ceramic sand > replacement rate of coal gangue ceramic particle > steel fiber content > polypropylene fiber content, which is also the same as the range analysis results, indicating that the analysis results are reliable.

To more intuitively reflect the influence of different factor levels on the experimental results, the intensity values in Table 4 were selected to draw the effect curve shown in Figure 3.

The maximum Y_i value corresponding to each factor is the optimal combination. According to Figure 3 and Table 4, for the compressive strength of cubes, the optimal combination is A2B2C3D2, that is, the replacement rate of coal gangue ceramics is 30%, the replacement rate of coal gangue ceramic sand is 30%, the content of steel fiber is 0.75%, and the content of polypropylene fiber

is 0.2%. For the splitting tensile strength, the optimal combination is A2B1C4D3, that is, the content of coal gangue ceramics is 30%, the replacement rate of coal gangue ceramic sand is 25%, the replacement rate of steel fiber is 1%, and the content of polypropylene fiber is 0.2%.

For factor A, the intensity increases first and then decreases. For factor B, the cube compressive strength increases first and then decreases, while the splitting tensile strength decreases. A comprehensive analysis of the relevant reasons can be seen:

Large holes in the coal gangue can improve its water absorption rate, resulting in a high degree of hydration around the coal gangue aggregate, forming an internal curing effect (Li et al., 2021). In addition, when the coal gangue is broken, coal gangue powder is adhered to the surface, which can promote the hydration reaction (Aslani et al., 2019a) and improve the strength of concrete. The promotion effect is recorded as P1 (Positive). The components of coal gangue contain a large amount of SiO_2 and Al_2O_3, which can be mixed with the hydration product $Ca(OH)_2$ of cement to produce a volcanic ash effect (Li et al., 2013; Duan, 2014; Li, 2014; Sun et al., 2021a), and the resulting network calcium silicate gel fills the gap between the aggregate itself and the aggregate, making the coal gangue aggregate more dense (Zhu et al., 2022). This promotion effect is recorded as P2. As the elastic modulus of coal gangue is lower than that of natural aggregate, the performance of coal gangue
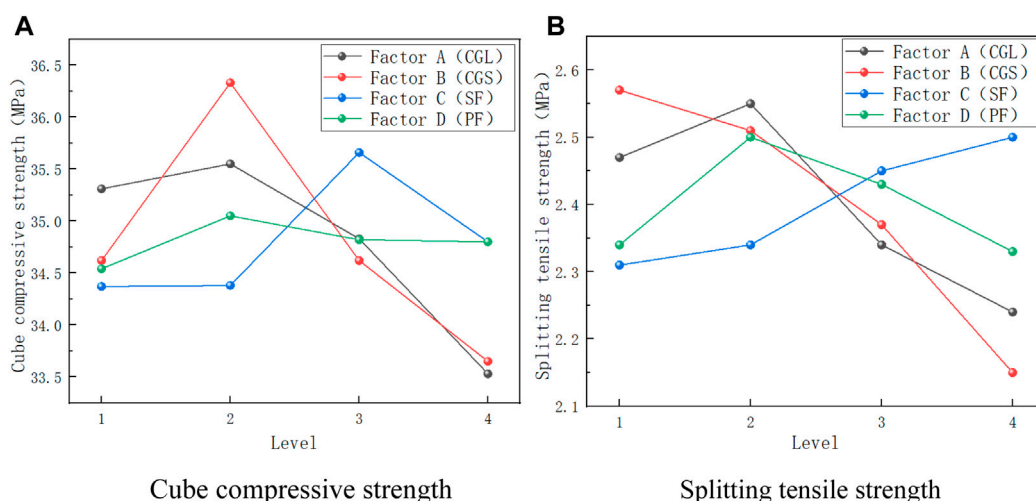
FIGURE 3
Range analysis effect curve.

FIGURE 4
Failure section of the specimen.

is poor. It can also be seen from the fracture surface in Figure 4 that the coal gangue itself is damaged. The research of Yan Bing (Yan, 2017a) and Chen Benpei (Chen, 1994) shows that when coal gangue concrete is damaged, coal gangue itself is damaged, which proves that the performance of coal gangue is inferior to that of natural aggregate. This weakening effect is denoted as H (Harmful). When P1 + P2 > H, that is, when the promoting effect is greater than the weakening effect, the strength of coal gangue concrete increases. When H > P1 + P2, that is, the weakening effect is greater than the promoting effect, the strength of coal gangue concrete decreases.

For factor C, the cube compressive strength increases first and then decreases, while the splitting tensile strength increases. For factor D, the intensity showed a trend of first

increasing and then decreasing, mainly for the following reasons:

The low-content steel-polypropylene fiber overlapped with each other in the concrete, resulting in a "hoop effect". When the concrete was damaged, more energy was consumed to pull out the fiber across the crack, thus restraining the rapid expansion of the crack. The macro performance was that the concrete strength was increased. When the content of steel-polypropylene fiber is increased, the fiber has an "agglomeration effect", which reduces the compactness of concrete. At this time, the weakening effect of the agglomeration effect is greater than the strengthening effect of the hoop effect, which shows that the strength of concrete decreases.

3.2 Grey correlation analysis

Grey correlation analysis is a quantitative description and comparison method for the development and change of a system. Its basic idea is to determine whether the reference data column is closely related by determining the similarity degree between the reference data column and several comparison data columns (Wu et al., 2022). The method introduced in the literature (Chen et al., 2023) was used to analyze the experimental results.

The cube compressive strength/splitting tensile strength was defined as the behavior sequence X_0 and factors A, B, C, and D were defined as factor sequences X_1, X_2, X_3, and X_4, respectively. The original data series obtained were shown in Table 8.

After initializing the original data, the correlation coefficient matrix as shown in Table 9 is obtained. In general, the greater the correlation coefficient, the greater the correlation degree; otherwise, the smaller the correlation degree. After the correlation coefficient is calculated according to the method described in the literature (Chen et al., 2023), the grey correlation degrees of different factors are obtained, as shown in Table 10.

As can be seen from Table 10, the correlation order is as follows: replacement rate of coal gangue ceramide > replacement rate of coal gangue ceramide > steel fiber content > polypropylene fiber content.

TABLE 8 SF-PF CGrc raw data series.

Cube compressive strength	Splitting tensile strength	X_1	X_2	X_3	X_4
X_0	X_0				
33.9000	2.3712	0.2500	0.2500	0.0025	0.0010
37.2000	2.6500	0.2500	0.3000	0.0050	0.0020
35.6554	2.4913	0.2500	0.3500	0.0075	0.0030
34.5014	2.3600	0.2500	0.4000	0.0100	0.0040
35.3000	2.8280	0.3000	0.2500	0.0050	0.0030
36.2800	2.4800	0.3000	0.3000	0.0025	0.0040
35.6400	2.5921	0.3000	0.3500	0.0100	0.0010
34.9700	2.3438	0.3000	0.4000	0.0075	0.0020
36.0300	2.5200	0.3500	0.2500	0.0075	0.0040
35.8400	2.4640	0.3500	0.3000	0.0100	0.0030
34.8000	2.4201	0.3500	0.3500	0.0025	0.0030
32.6300	1.9521	0.3500	0.4000	0.0050	0.0010
33.2362	2.5800	0.4000	0.2500	0.0100	0.0020
35.9810	2.4600	0.4000	0.3000	0.0075	0.0010
32.4000	1.9592	0.4000	0.3500	0.0050	0.0040
32.5000	1.9583	0.4000	0.4000	0.0025	0.0030

TABLE 9 Correlation coefficient matrix of SF-PF CGrc.

Cube compressive strength				Splitting tensile strength			
Y1(k)	Y2(k)	Y3(k)	Y4(k)	Y1(k)	Y2(k)	Y3(k)	Y4(k)
1.0000	1.0000	1.0000	1.0000	1.0000	1.0000	1.0000	1.0000
0.9399	0.9368	0.6277	0.6277	0.9307	0.9509	0.6427	0.6427
0.9671	0.8138	0.4386	0.4386	0.9691	0.8195	0.4487	0.4487
0.9885	0.7233	0.3379	0.3379	0.9973	0.7242	0.3456	0.3456
0.9056	0.9736	0.6136	0.4373	0.9884	0.8974	0.6596	0.4659
0.9214	0.9214	0.9559	0.3419	0.9117	0.9117	0.9716	0.3494
0.9110	0.8136	0.3405	0.9674	0.9367	0.8378	0.3531	0.9447
0.9004	0.7281	0.4361	0.6112	0.8818	0.7214	0.4408	0.6104
0.8187	0.9604	0.4400	0.3413	0.8249	0.9616	0.4503	0.3507
0.8162	0.9142	0.3409	0.4393	0.8142	0.9073	0.3488	0.4471
0.8030	0.8030	0.9829	0.4354	0.8072	0.8072	0.9869	0.4450
0.7768	0.7048	0.5947	0.9760	0.7332	0.6712	0.5740	0.8995
0.7107	0.9873	0.3351	0.5989	0.7562	0.9471	0.3527	0.6351
0.7386	0.9165	0.4398	0.9612	0.7384	0.9073	0.4471	0.9766
0.7026	0.7741	0.5931	0.3333	0.6724	0.7347	0.5749	0.3333
0.7036	0.7036	0.9736	0.4272	0.6724	0.6724	0.9017	0.4220

The degree of influence of different factors on the test results can be obtained by analyzing the degree of correlation. The degree of influence from strong to weak is the replacement rate of coal gangue ceramic sand, the replacement rate of coal gangue ceramic particles, the content of steel fiber, and the content of polypropylene fiber. This is also consistent with the analysis results in Section 3.1, indicating that the test results are reliable.

According to the test results, the optimal mix ratio of hybrid fiber coal gangue concrete is 30% replacement rate of coal gangue ceramide, 25%–30% replacement rate of coal gangue ceramide sand, 0.75%–1% steel fiber content and 0.1% polypropylene fiber content.

3.3 Establishment and detection of grey model GM (1, 5)

The grey model is to generate a new regular array of some irregular data through mathematical operation, establishes a differential equation, and calculates the coefficient by the least square method. The multi-variable GM (1, N) model is the extension of n-element variables under the GM (1, 1) model, which reflects the influence of n-1 variables on the first derivative of a variable (Sun et al., 2022a; Zhang et al., 2022c; Zhang et al., 2023b).

3.3.1 The establishment of grey model GM (1, 5)
When building a GM model, it is necessary to build the original sequence first, and the original sequence that meets the modeling

TABLE 10 Grey correlation degree of SF-PF CGrc.

Performance	Coal gangue ceramide content (γ_1)	Coal gangue ceramic sand content (γ_2)	Steel fiber content (γ_3)	Polypropylene fiber content (γ_4)
Cube compressive strength	0.850	0.855	0.591	0.580
Splitting tensile strength	0.842	0.852	0.594	0.582

TABLE 11 GM(1, 5) Original sequence X(n) of cube compressive strength.

Feature sequence	Correlation behavior sequence			
X_0	X_1	X_2	X_3	X_4
1.76171	1.61441	1.61441	1.60949	1.60946
1.80815	1.61441	1.61540	1.60954	1.60948
1.78695	1.61441	1.61639	1.60959	1.60950
1.77050	1.61441	1.61737	1.60964	1.60952
1.78194	1.61540	1.61441	1.60954	1.60950
1.79563	1.61540	1.61540	1.60949	1.60952
1.78673	1.61540	1.61639	1.60964	1.60946
1.77725	1.61540	1.61737	1.60959	1.60948
1.79218	1.61639	1.61441	1.60959	1.60952
1.78953	1.61639	1.61540	1.60964	1.60950
1.77481	1.61639	1.61639	1.60949	1.60950
1.74262	1.61639	1.61737	1.60954	1.60946
1.75182	1.61737	1.61441	1.60964	1.60948
1.79150	1.61737	1.61540	1.60959	1.60946
1.73908	1.61737	1.61639	1.60954	1.60952
1.74062	1.61737	1.61737	1.60949	1.60950

TABLE 12 GM (1, 5)Original sequence X(n) of splitting tensile strength.

Feature sequence	Correlation behavior sequence			
X_0	X_1	X_2	X_3	X_4
0.43170	0.40547	0.40547	0.34720	0.34682
0.48728	0.40547	0.41645	0.34782	0.34707
0.45640	0.40547	0.42721	0.34845	0.34732
0.42933	0.40547	0.43773	0.34907	0.34757
0.51978	0.41645	0.40547	0.34782	0.34732
0.45413	0.41645	0.41645	0.34720	0.34757
0.47623	0.41645	0.42721	0.34907	0.34682
0.42589	0.41645	0.43773	0.34845	0.34707
0.46213	0.42721	0.40547	0.34845	0.34757
0.45089	0.42721	0.41645	0.34907	0.34732
0.44190	0.42721	0.42721	0.34720	0.34732
0.33445	0.42721	0.43773	0.34782	0.34682
0.47389	0.43773	0.40547	0.34907	0.34707
0.45008	0.43773	0.41645	0.34845	0.34682
0.33627	0.43773	0.42721	0.34782	0.34757
0.33604	0.43773	0.43773	0.34720	0.34732

needs to meet the principle of smoothness or quasi-smoothness. The sufficient and necessary conditions for determining whether the original sequence is smooth are $\forall \varepsilon > 0$, $\exists k_0$, $\rho(k) < \varepsilon$ when $k > k_0$, where ε is a constant, k_0 is the number of experimental groups, $\rho(k)$ is the smooth ratio.

After testing, it is necessary to change the digital-power function complex operator of formula (1) on the original sequence. Meanwhile, to ensure the tidiness of the transformed results, the original sequence needs to be transformed by formula (2) first for the cube compressive strength, and by formula (3) for the splitting tensile strength. The original sequence X(n) after transformation is shown in Tables 11, 12.

$$x(k)d = \ln x(k)^{0.5} \qquad (1)$$
$$x(k)d = x(k) + 25 \qquad (2)$$
$$x(k)d = x(k) + 2 \qquad (3)$$

GM (1, 5) models of compressive strength and splitting tensile strength of SF-PF CGrc were established as follows:

$$\frac{dx}{dt} + ax_1 = b_1 x_2 + b_2 x_3 + b_3 x_4 + b_4 x_5 \qquad (4)$$

Where, x_1, x_2, x_3, x_4, x_5 are respectively cube compressive strength/splitting tensile strength, replacement rate of coal gangue ceramide, replacement rate of coal gangue ceramic sand, steel fiber content and polypropylene fiber content, a is the system development coefficient, b_1, b_2, b_3, b_4 is the driving coefficient

The original sequence after transformation is accumulated and generated according to formula (5), and then the system development coefficient (D) and driving term coefficient () are calculated according to formulas (6)~(8), and the calculated values are brought into formula (4) to obtain the parameter values, and the parameter results are shown in Table 13.

$$x_i^{(1)}(k) = \sum_{l=1}^{k} x_i^{(0)}(l) \qquad (5)$$

TABLE 13 GM (1, 5) model parameters.

Parameters	a	b_1	b_2	b_3	b_4
Cube compressive strength	1.8766	−24.0665	−23.9767	121.7039	−71.4018
Splitting tensile strength	1.1933	−3.6466	−5.6907	27.9568	−15.1711

The resulting cube compressive strength estimation model is as follows:

$$D = \begin{bmatrix} -\frac{1}{2}\left[X_1^{(1)}(1) + X_1^{(1)}(2)\right] & X_2^{(1)}(2) & \cdots & X_4^{(1)}(2) \\ -\frac{1}{2}\left[X_1^{(1)}(2) + X_1^{(1)}(3)\right] & X_1^{(1)}(3) & \cdots & X_4^{(1)}(3) \\ \vdots & \vdots & \ddots & \vdots \\ -\frac{1}{2}\left[X_1^{(1)}(15) + X_1^{(1)}(16)\right] & X_1^{(1)}(16) & \cdots & X_4^{(1)}(16) \end{bmatrix} \quad (6)$$

$$D = \begin{bmatrix} X_1^{(0)}(2) \\ X_1^{(0)}(3) \\ \vdots \\ X_1^{(0)}(16) \end{bmatrix} \quad (7)$$

$$\hat{a} = \begin{bmatrix} a & b_1 & b_2 & b_3 \end{bmatrix}^T = (D^T D)^{-1} D^T Y \quad (8)$$

$$\frac{dx}{dt} + 1.8766x_1 = -24.0665x_2 - 23.9767x_3 + 121.7039x_4 - 71.4018x_5 \quad (9)$$

The resulting splitting tensile strength estimation model is as follows:

$$\frac{dx}{dt} + 1.1933x_1 = -3.6466x_2 - 5.6907x_3 + 27.9568x_4 - 15.1711x_5 \quad (10)$$

Formula (10) is transformed into a cube compressive strength prediction model. The standard formula is:

$$X(t+1) = [1.76171 + 12.824x_2 + 12.777x_3 - 64.853x_4 + 38.048x_5]e^{-1.8766t} \\ -12.824x_2 - 12.777x_3 + 64.853x_4 - 38.048x_5 \quad (11)$$

Formula (11) is transformed into a splitting tensile strength prediction model. The standard formula is:

$$X(t+1) = [0.4317 + 3.056x_2 + 4.769x_3 - 23.428x_4 + 12.714x_5]e^{-1.1933t} \\ -3.056x_2 - 4.769x_3 + 23.428x_4 - 12.714x_5 \quad (12)$$

3.3.2 Grey prediction model GM (1,5) results

The strength prediction model of SF-PF CGrc was used to predict and evaluate 16 groups of test data, and the results were tested by residual test to determine the accuracy of the model. The comparison of test values and model predicted values of cube compressive strength and splitting tensile strength is shown in Table 14.

To more intuitively observe the error between the test value and the predicted value, the test value and the predicted value were drawn as a comparison curve as shown in Figure 5. Due to the certain discreteness of the cube specimens during the test, there were large errors in some groups. It shows that the prediction effect of the model is good. In the horizontal range selected in this paper, the cubic compressive strength

and splitting tensile strength of SF-PF CGrc can be predicted, which provides theoretical support for the strength prediction of SF-PF CGrc.

4 Microstructure analysis of steel-polypropylene fiber coal gangue concrete

The interfacial transition zone (ITZ) will be formed when coal gangue and fiber are mixed into the concrete matrix. The different failure modes of materials and the evolution process of ITZ have an important influence on the strength of concrete.

In this paper, 4 samples were selected from the fracture surface of the specimen to observe the ITZ, and coal gangue ceramic particles, ceramic sand, and polypropylene fiber were selected to observe the original appearance of the material. After gold spraying by a plasma sputtering instrument, they were placed under an S-3400 electron microscope to observe their microscopic morphology, as shown in Figure 6.

4.1 Micromorphology and destruction mode of fiber and coal gangue

4.1.1 Microstructure and destruction mode of fiber

Figure 7A is the microscopic morphology of polypropylene fiber 500 times magnification, the fiber surface is smoother, and the cement slurry wraps less (Wang et al., 2023), so the bonding strength at the interface connection is low when the specimen is under load, polypropylene fiber is easy to be pulled out, Figure 7B is the trace left by the polypropylene fiber being pulled out.

Combining the results of range analysis and variance analysis, the polypropylene fiber can improve the tensile strength of concrete, for the compressive strength of concrete, the role of polypropylene fiber is small. Therefore, when the content of polypropylene fiber is too high, it will also reduce the compactness of concrete, resulting in a decrease in concrete strength.

Figure 7C is the micromorphology of steel fiber, its surface is rougher, cement slurry can be well-wrapped steel fiber, and the surface distribution of hydration product particles of steel fiber also confirms the above situation, as shown in Figure 7D good wrapping increases the bonding effect between steel fiber and concrete matrix when subjected to an external load, it takes more energy to pull or pull out the steel fiber, macroscopically manifested as steel fiber can significantly improve the strength of concrete.

4.1.2 Micromorphology and destruction mode of coal gangue

The overall structure of coal gangue is looser than that of natural stone (Di et al., 2016), and there are a large number of micro-pores in the coal gangue ceramics and sand. Figure 8A is 250 times larger than

TABLE 14 Comparison of experimental values and model predicted values.

Specimen number	Cube compressive strength				Splitting tensile strength			
	Experimental value (MPa)	Predicted value (MPa)	Residual error (MPa)	Relative error (%)	Experimental value (MPa)	Predicted value (MPa)	Residual error (MPa)	Relative error (%)
A1B1C1D1	33.90	33.90	0.00	0.00	2.37	2.37	0.08	7.70
A1B2C2D2	37.20	34.36	2.84	8.28	2.65	2.46	−0.05	4.90
A1B3C3D3	35.66	38.89	−3.24	8.32	2.49	2.62	−0.02	2.35
A1B4C4D4	34.50	38.71	−4.20	10.86	2.36	2.42	−0.06	6.28
A2B1C2D3	35.30	37.86	−2.56	6.75	2.83	3.02	−0.03	2.68
A2B2C1D4	36.28	35.73	0.55	1.54	2.48	2.55	0.03	2.70
A2B3C4D1	35.64	34.80	0.84	2.42	2.59	2.52	0.07	6.95
A2B4C3D2	34.97	34.31	0.66	1.93	2.34	2.19	−0.08	8.40
A3B1C3D4	36.03	33.87	2.16	6.37	2.52	2.75	−0.04	3.94
A3B2C4D3	35.84	34.51	1.33	3.86	2.46	2.57	0.14	14.13
A3B3C1D2	34.80	33.80	1.00	2.94	2.42	2.12	−0.06	6.04
A3B4C2D1	32.63	33.27	−0.64	1.94	1.95	2.08	−0.04	3.98
A4B1C4D2	33.24	35.40	−2.17	6.12	2.58	2.69	0.04	4.01
A4B2C3D1	35.98	34.35	1.63	4.75	2.46	2.37	−0.04	3.68
A4B3C2D4	32.40	33.79	−1.39	4.12%	1.96	2.03	0.09	8.92%
A4B4C1D3	32.50	29.67	2.83	9.55%	1.96	1.80	2.83	9.55%
Mean relative error	4.98%				5.42%			

FIGURE 5
Comparison graph of test values and model predicted values.

FIGURE 6
Test instrument and sample.

FIGURE 7
Micromorphology and destruction forms of fibers. **(A)** Microstructure of polypropylene fiber. **(B)** Damage form of polypropylene fiber. **(C)** Microstructure of steel fiber. **(D)** Failure form of steel fiber.
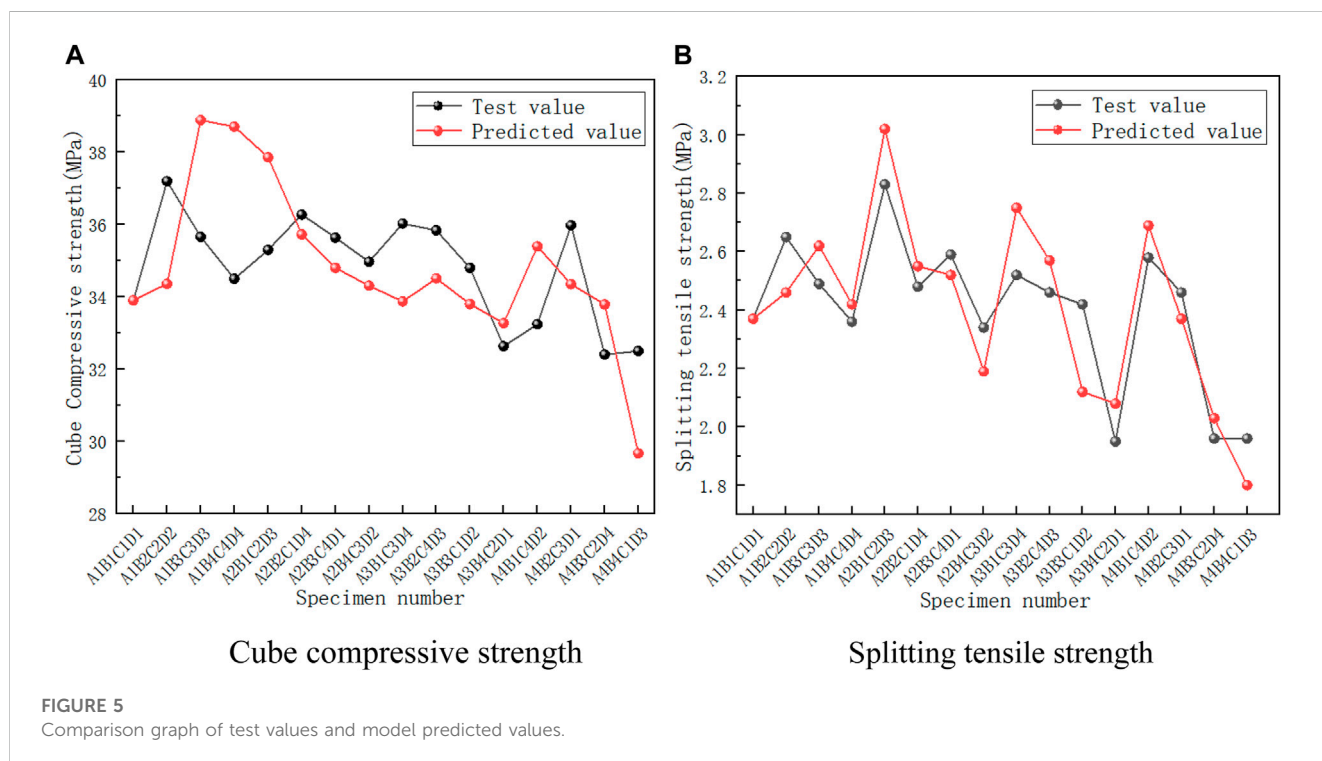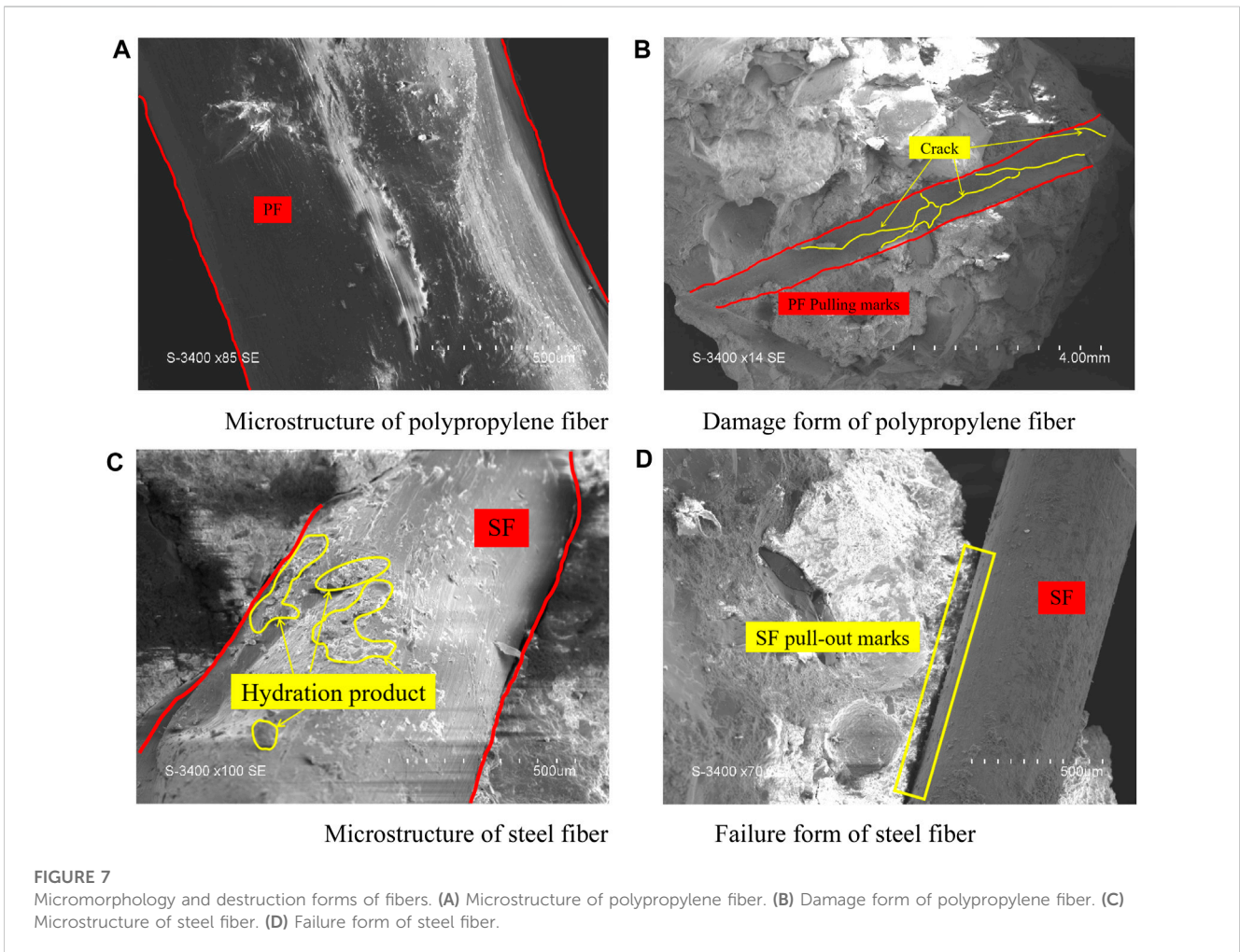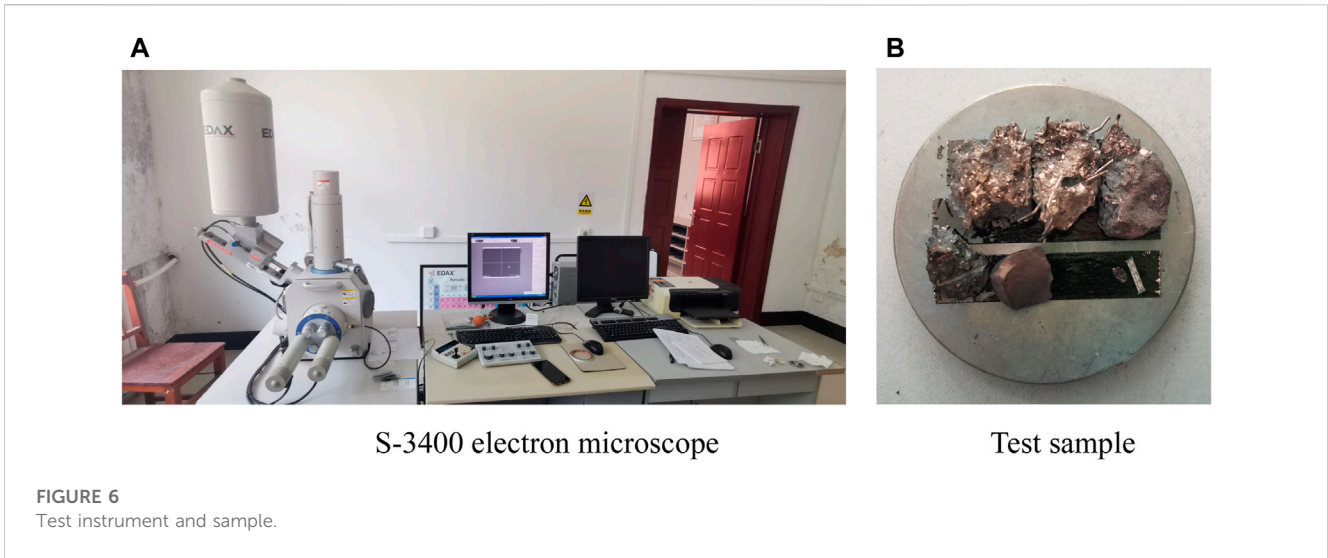
the fracture surface of coal gangue, and it can be seen that the fracture surface is distributed with holes of different sizes. In addition, cement hydration products and sand particles of different sizes and shapes are attached to the fracture surface. It can also be observed in Figure 8B that coal gangue sand is attached to the aggregate surface. Since the stiffness of the sand is lower than that of natural fine aggregate, when the concrete is subjected to load, cracks appear in the concrete, and coal gangue sand also breaks. Therefore, the strength of SF-PF CGrc decreases with high coal gangue content.
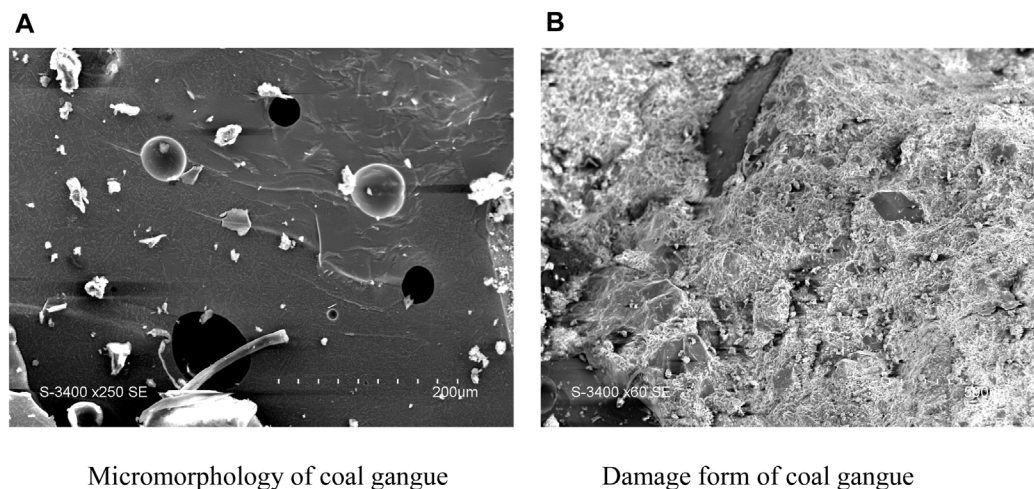
FIGURE 8
Microstructure of coal gangue and its failure form. **(A)** Micromorphology of coal gangue **(B)** Damage form of coal gangue.

4.2 Formation mechanism and microstructure of interfacial transition zone

The formation of an interfacial transition zone (ITZ) is not only due to the accumulation of particles along the aggregate surface and the result of hydration reaction but is also affected by many factors such as stirring and curing, so it can be observed by SEM. The ITZ formation mechanism and micro-morphology of SF-PF CGrc were investigated to provide a theoretical basis for the study of the mechanical properties of SF-PF CGrc.

4.2.1 Formation mechanism of interfacial transition zone

The structure at ITZ inside concrete is relatively loose and prone to micro-cracks, which seriously affects the performance of concrete. Currently, the generally accepted ITZ formation mechanism mainly includes wall effect, micro bleeding or localized bleeding, ion transportation, precipitation and nucleation, one-side growth, flocculation of binder, and syneresis. These mechanisms reveal the formation process of ITZ from different levels and provide a theoretical basis for explaining the changes in different stages of ITZ formation.

4.2.1.1 Wall effect

Using electron microscopy, Berger et al. (1970) observed that cement was randomly distributed in the matrix, and aggregate, as an impenetrable physical constraint, prevented the dispersion of cement particles (Aslani et al., 2019b; Luo et al., 2021). The intervention of aggregate made small particles near the aggregate surface dominate, while large particles occupied the main position in the area far away from the aggregate surface (Wang et al., 2021). as Shown in Figure 9. Fang and Zhang (2020) showed that the particle size of cement particles located in ITZ was 0.5~11.5 μm, while the particle size of cement particles in the matrix part was 2.5~62.5 μm. Therefore, there are a large number of loose porous structures around the aggregate (Ma and Li, 2014), and the porosity of ITZ at 3 μm from the aggregate surface reaches 25%, while the porosity of cement slurry is 8% (Branch et al., 2018). Finally, the porosity of ITZ increases, and the deterioration rate of concrete accelerates (He et al., 2020).

4.2.1.2 Microbleeding or localized bleeding

The main reason for the micro-zone bleeding effect is the density difference between cementing material, coarse aggregate, and water. During the vibration process, the cementing material moves downward, and the aggregate obstructs the upward migration of water, causing water to accumulate in the area near the lower surface of the aggregate and form a water film (Shi et al., 2016) as in Figure 10 The micro-zone bleeding effect plays a major role in the ITZ formation of concrete with a high water-cement ratio, and with the increase of the water-cement ratio, the micro-zone bleeding effect of concrete becomes more obvious (Liu et al., 2019).

4.2.1.3 Ion transportation, precipitation and nucleation

In the hydration process of the gelling material, the solubility of each component and the migration rate of ions vary greatly and change with the hydration process. The silicon-containing components in the particles of the gelling material are rapidly deposited on the surface of the particles of the gelling material to form hydration products (Stroeven and Stroeven, 2001), and most of the Ca^{2+}, SO_4^{2-}, OH^-, and Al^{3+} enter the solution. Aggregate near the surface of the aggregate and combine, depositing and nucleating in the form of AFt (ettringite) and CH (calcium hydroxide) (Xuan et al., 2009).

4.2.1.4 One-side growth

In the slurry, C-S-H (hydrated calcium silicate) produced by the hydration reaction of the cementing material can grow from all directions to any area, but in the area near the aggregate, the hydration product can only grow to one side of the cement slurry, resulting in unilateral growth effect (Gartner et al., 2000). The unilateral growth effect weakens the cohesiveness between aggregate and slurry and reduces the mechanical properties of ITZ (Ghourchian et al., 2018a).

4.2.1.5 Flocculation of binder

Under the action of van der Waals force and static electricity, the particles in the dispersion grow in the form of clusters, causing the flocculation effect (Thomas and Jennings, 2006). The surface
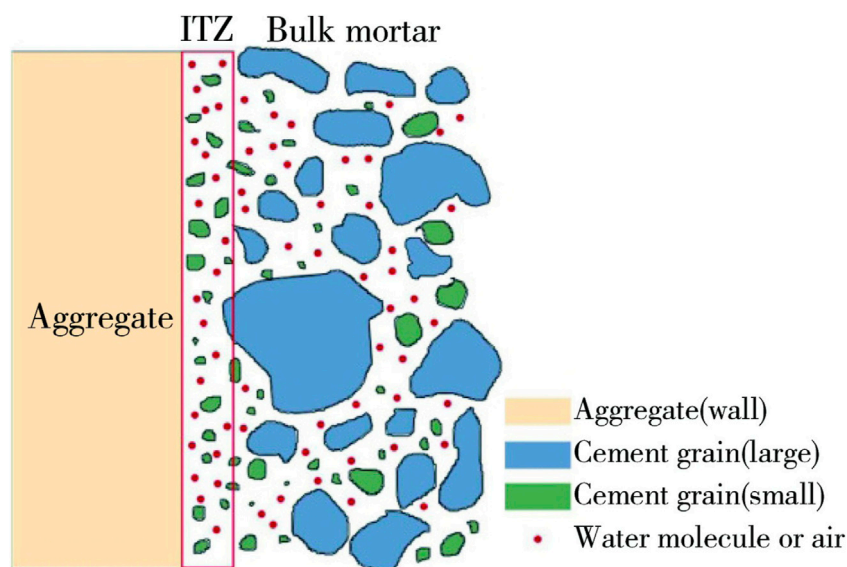
FIGURE 9
Diagram of wall effect (Wang et al., 2021).
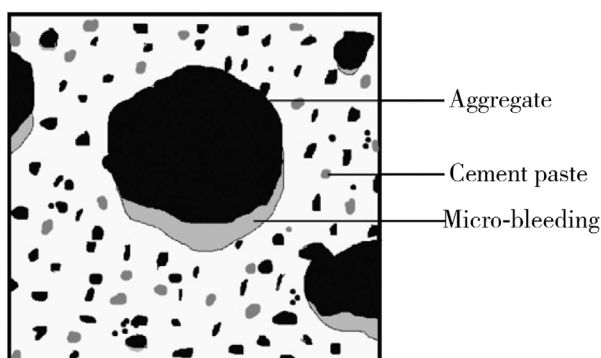
FIGURE 10
Diagram of microbleeding or localized bleeding (Shi et al., 2016).

charges of the cement particles cancel each other, reducing the previous repulsion of the particles (Ghourchian et al., 2018a). At the same time, the high specific surface area and hydration activity of cement lead to the flocculation effect, which reduces the cement packing density around the aggregate and forms loose porous ITZ.

4.2.1.6 Syneresis

In the process of cementitious materials, colloidal particles overlap into clumps with each other, and there is a solvent wrapped inside the group, and the glue will inevitably shrink to reduce its potential energy, so the encapsulated solvent will be eliminated from the inside of the glue. The overall manifestation is that the solvent is discharged, but the volume of the entire system remains unchanged (Wilhelm and Kind, 2015). In addition, because the aggregate does not shrink, the slurry and the aggregate cannot shrink and deform at the same time, which leads to tensile stress

inside the concrete, and it is easy to form microcracks between the aggregate and the cement slurry (Szeląg and Fic, 2016).

4.2.2 Microstructure of interfacial transition zone
4.2.2.1 Microstructure of the transition zone between fiber and cement slurry

The SEM image of the transition zone between steel fiber and cement slurry in Figure 11A shows the distribution of materials. Because the steel fibers distributed randomly are overlapping with each other in concrete, the hoop effect is formed, which reduces the sinking of aggregate and enhances the performance of ITZ. These hydration products can be bonded with steel fibers, and when the steel fibers are subjected to load, more energy is consumed, that is, a certain strengthening and toughening effect is achieved.

Due to the smooth surface of polypropylene fiber, the shrinkage of the cement base in the curing process will lead to the separation of pulp on the fiber surface, which will affect the hydration reaction degree of the cement base near the surface. At the same time, due to the hydrophobicity of polypropylene fiber, there is no excess water accumulation on the surface of the fiber, resulting in the hydration of cement near the interface transition zone to form low-density C-S-H (Sun et al., 2021b; Sun et al., 2022b), as shown in Figure 11B.

4.2.2.2 Microstructure of transition zone between coal gangue and cement slurry

As can be seen from Figure 12, the surface of coal gangue consists of many different types of hydration products, and many cracks and pores after fiber drawing can be observed on the surface of the matrix. With the increase of curing time, the hydration of substances in the matrix becomes more thorough, the hydration products increase significantly, and AFt and CH generated by hydration expand with the deepening of hydration degree, filling the micro holes and cracks in the matrix, making the material bond again, and enhancing the strength of concrete. In addition, due to
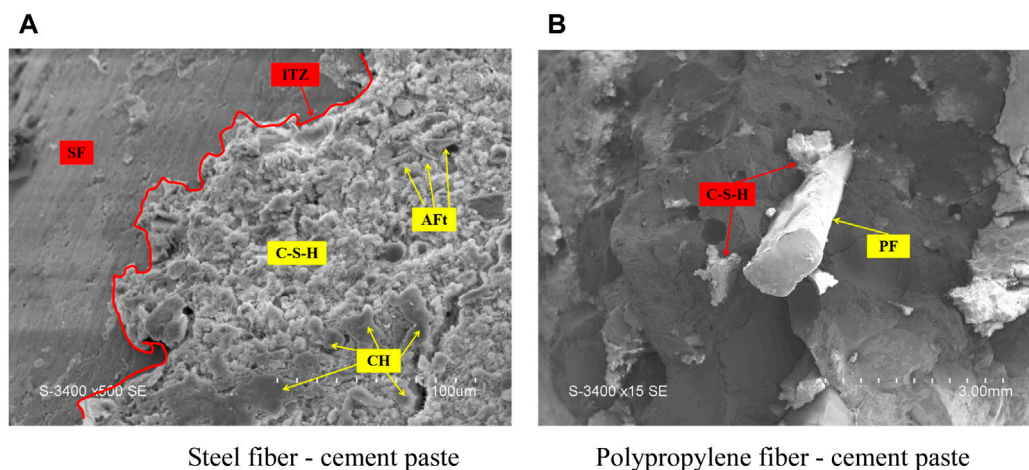
FIGURE 11
Fiber—water slurry interface transition zone microstructure. **(A)** Steel fiber—cement paste. **(B)** Polypropylene fiber—cement paste.
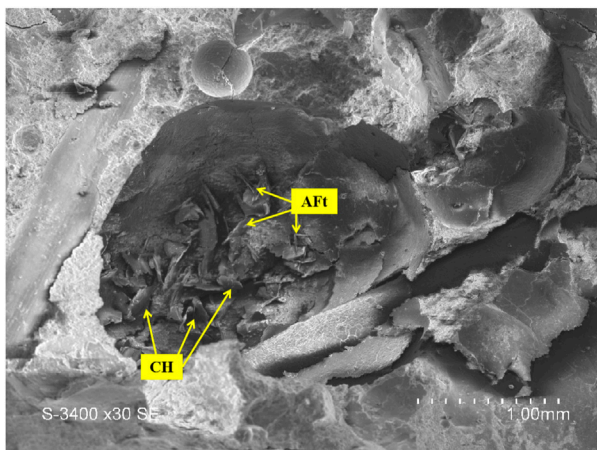
FIGURE 12
Coal—water slurry interface transition zone microstructure.

the irregular surface of coal gangue and the adhesion of active coal gangue powder, the coating area with cement slurry is increased, the hydration reaction is further strengthened, and the mechanical properties of SF-PF CGrc are improved to a certain extent.

5 Conclusion

Through the orthogonal test of SF-PF CGrc, the influence of coal gangue and fiber on the mechanical properties of concrete was studied, and combined with the microscopic analysis, the research conclusions were as follows:

(1) The strength of hybrid fiber concrete specimens is significantly greater than that of ordinary concrete specimens, and the cube compressive strength is increased by 24.62% and the splitting tensile strength is increased by 57.3% compared with PC.

(2) Range analysis and variance analysis were carried out on the specimens, and it was concluded that the significant degree of influence of each factor on the cubic compressive strength and splitting tensile strength of concrete was ranked from strong to weak as follows: Coal gangue sand content > coal gangue clay content > steel fiber content > polypropylene fiber content, and the optimal content is coal gangue clay replacement rate of 30%, coal gangue clay replacement rate of 30%, steel fiber content of 0.75%, polypropylene fiber content of 0.2%. The results of the grey correlation analysis are also consistent with them, and the strength of the steel fiber coal gangue concrete prepared can reach C30.

(3) The grey prediction model for the compressive strength and splitting tensile strength of hybrid fiber coal gangue concrete was established. The relative error of the test value and the predicted value was tested. The average relative error of the test value and the predicted value of the model was 4.98%/5.42%, indicating that the prediction accuracy of the model was high.

(4) The poor stiffness of coal gangue leads to a decline in strength. After the addition of steel fiber and polypropylene fiber, the formed three-dimensional skeleton can improve the stability of the interfacial transition zone, and the formed C-S-H and AFt fill microholes and cracks to bond the materials together, enhance the compactness of the matrix and improve the strength of concrete.

Data availability statement

The original contributions presented in the study are included in the article/Supplementary Material, further inquiries can be directed to the corresponding author.

Author contributions

JL: Conceptualization, Formal Analysis, Funding acquisition, Writing–review and editing. LC: Conceptualization, Formal

Analysis, Writing–original draft, Writing–review and editing. JL: Methodology, Validation, Writing–review and editing. YZ: Formal Analysis, Methodology, Resources, Writing–review and editing. XF: Formal Analysis, Writing–review and editing. GH: Project administration, Writing–review and editing.

Conflict of interest

The authors declare that the research was conducted in the absence of any commercial or financial relationships that could be construed as a potential conflict of interest.

Publisher's note

All claims expressed in this article are solely those of the authors and do not necessarily represent those of their affiliated organizations, or those of the publisher, the editors and the reviewers. Any product that may be evaluated in this article, or claim that may be made by its manufacturer, is not guaranteed or endorsed by the publisher.

References

Afroughsabet, V., and Ozbakkaloglu, T. .Mechanical and durability properties of high-strength concrete containing steel and polypropylene fibers.Constr. Build. Mater., 2015, 94:73–82. doi:10.1016/j.conbuildmat.2015.06.051

Aslani, F., Sun, J., Bromley, D., and Ma, G. Fiber-reinforced lightweight self-compacting concrete incorporating scoria aggregates at elevated temperatures." Struct. Concr. 20 (2019b): 1022–1035. doi:10.1002/suco.201800231

Aslani, F., Sun, J., and Huang, G. "Mechanical behavior of fiber-reinforced self-compacting rubberized concrete exposed to elevated temperatures." J. Mater. Civ. Eng. 31 (2019a): 04019302, doi:10.1061/(asce)mt.1943-5533.0002942

Berger, R. L., Cahn, D. S., and McGregor, J. D. Calcium hydroxide as a binder in Portland cement paste. J. Am. Ceram. Soc., 1970, 53(1): 57–58. doi:10.1111/j.1151-2916.1970.tb12004.x

Branch, J. L., Epps, R., and Kosson, D. S. The impact of carbonation on bulk and ITZ porosity in microconcrete materials with fly ash replacement. Cem. Concr. Res., 2018, 103: 170–178. doi:10.1016/j.cemconres.2017.10.012

Chen, B. Strength of coal gangue concrete. Ind. Build.,1994(07):29–32+42.

Chen, N., Sun, Y., Wang, Z., et al. Identification of flight accidents causative factors base on SHELLO and improved entropy gray correlation method. Heliyon, 2023. doi:10.1016/j.heliyon.2023.e13534

China Academy of Building Research. General concrete mix design code: jgj 55-2011 [S]. Beijing: China Building and Construction Press, 2011.

Di, W., Zhang, Y., and Liu, Y. Mechanical performance and ultrasonic properties of cemented gangue backfill with admixture of fly ash. Ultrasonics, 2016, 64:89–96. doi:10.1016/j.ultras.2015.08.004

Duan, X. Research on microstructure and physical and mechanical properties of coal gangue aggregate concrete [D]. China, China University of Mining and Technology,2014.

Fang, G., and Zhang, M. Multiscale micromechanical analysis of alkali-activated fly ash-slag paste. Cem. Concr. Res., 2020, 135: 106141, doi:10.1016/j.cemconres.2020.106141

Feng, W., Wang, Y., Sun, J., Tang, Y., Wu, D., Jiang, Z., et al. 2022, . Prediction of thermo-mechanical properties of rubber-modified recycled aggregate concrete." Constr. Build. Mater. 318 (2022): 125970, doi:10.1016/j.conbuildmat.2021.125970

Gartner, E. M., Kurtis, K. E., and Monteiro, P. J. M. Proposed mechanism of CSH growth tested by soft X-ray microscopy. Cem. Concr. Res., 2000, 30(5): 817–822. doi:10.1016/s0008-8846(00)00235-0

Ghourchian, S., Wyrzykowski, M., Baquerizo, L., and Lura, P. Performance of passive methods in plastic shrinkage cracking mitigation. Cem. Concr. Compos., 2018a, 91: 148–155. doi:10.1016/j.cemconcomp.2018.05.008

Guan, H., Yu, J., Wang, J., and Pi, J. Experimental and analytical model of CFRP-confined spontaneous combustion coal gangue aggregate concrete. Constr. Build. Mater., 2023, 404: 133261, doi:10.1016/j.conbuildmat.2023.133261

He, R., Zheng, S., Gan, V. J. L., Wang, Z., Fang, J., and Shao, Y. Damage mechanism and interfacial transition zone characteristics of concrete under sulfate erosion and Dry-Wet cycles. Constr. Build. Mater., 2020, 255: 119340, doi:10.1016/j.conbuildmat.2020.119340

Huang, C. Research on seepage resistance and frost resistance of concrete with coal gangue replacing coarse aggregate. Shenyang, Shenyang Jianzhu University,2015.

Huang, G., Ji, Y., Li, J., Hou, Z., and Dong, Z. Improving strength of calcinated coal gangue geopolymer mortars via increasing calcium content. Constr. Build. Mater.,2018,166, 760–768. doi:10.1016/j.conbuildmat.2018.02.005

Institute of Standard Quotas, Ministry of Housing and Urban-Rural Development. Steel fiber reinforced concrete: jg/T472-2015[S]. Beijing: Standards Press of China, 2015.

Li, J., Chen, L., Luo, J., Zhu, W., Fan, X., Zhu, Y., et al. 2023a, Mechanical properties and microscopic characteristics of steel fiber coal gangue concrete. Front. Mater. 10: 1211129.doi:10.3389/fmats.2023.1211129

Li, J., Chen, L., Wang, X., Hu, G., Wang, Z., Guo, J., et al. Effect of compounding conductive materials on the mechanical properties of concrete and the microscopic mechanism. Constr. Build. Mater., 377, 2023b: 131000, doi:10.1016/j.conbuildmat.2023.131000

Li, J., Qin, Q., Sun, J., Ma, Y., and Li, Q. Mechanical and conductive performance of electrically conductive cementitious composite using graphite, steel slag, and GGBS." Struct. Concr. 23. (2022b): 533–547. doi:10.1002/suco.202000617

Li, J., Zhao, E., Niu, J., and Wan, C. Study on mixture design method and mechanical properties of steel fiber reinforced self-compacting lightweight aggregate concrete. Constr. Build. Mater., 2021, 267: 121019, doi:10.1016/j.conbuildmat.2020.121019

Li, M. Research on performance of high performance coal gangue concrete [D]. Shenyang, Shenyang Jianzhu University,2014.

Li, S., Zhou, M., and Zhang, L. 2022a, Characteristics of coarse aggregate of spontaneous combustion coal gangue and its effect on concrete properties. J. Build. Mater.,2023(02):334–340+380.

Li, Y., Yao, Y., Liu, X., Sun, H., and Ni, W. Improvement on pozzolanic reactivity of coal gangue by integrated thermal and chemical activation. Fuel, 2013, 109:527–533. doi:10.1016/j.fuel.2013.03.010

Liang, X., Wang, S., and Li, X. Principles of concrete structure design - 2nd Edition Science Press, 2007.

Liu, H., Bai, G., Gu, Y., and Yan, F. The influence of coal gangue coarse aggregate on the mechanical properties of concrete columns. Case Stud. Constr. Mater., 2022, 17: e01315, doi:10.1016/j.cscm.2022.e01315

Liu, R., Xiao, H., Liu, J., Guo, S., and Pei, Y. Improving the microstructure of ITZ and reducing the permeability of concrete with various water/cement ratios using nano-silica. J. Mater. Sci., 2019, 54(1): 444–456. doi:10.1007/s10853-018-2872-5

Luo, Z., Li, W., Wang, K., Castel, A., and Shah, S. P. Comparison on the properties of ITZs in fly ash-based geopolymer and Portland cement concretes with equivalent flowability. Cem. Concr. Res., 2021, 143: 106392, doi:10.1016/j.cemconres.2021.106392

Ma, H., and Li, Z. Multi-aggregate approach for modeling interfacial transition zone in concrete. ACI Mater. J., 2014, 111(2): 189. doi:10.14359/51686501

Ministry of Construction of the People's Republic of China. Test method standard for mechanical properties of ordinary concrete: GB/T50081-2016[S]. Beijing China Architecture and Construction Press, 2016.(in Chinese)

Qiu, J., Zhang, R., Guan, X., Cheng, K., Gao, Y., and Xiao, Z. Deterioration characteristics of coal gangue concrete under the combined action of cyclic loading and freeze-thaw cycles. J. Build. Eng., 2022, 60: 105165, doi:10.1016/j.jobe.2022.105165

Shi, H., Sun, D., and Wu, K. Microstructure and interface transition zone of concrete. Res. Prog. Numer. Simul. method Silic. sinica, 2016, 44 (5) : 678–685. doi:10.14062/j.iSSN.0454-5648.2016.05.10

Stroeven, P., and Stroeven, M. Reconstructions by SPACE of the interfacial transition zone. Cem. Concr. Compos., 2001, 23(2-3): 189–200. doi:10.1016/s0958-9465(00)00076-7

Sun, J., Wang, J., Zhu, Z., He, R., Peng, C., Zhang, C., et al. Mechanical performance prediction for sustainable high-strength concrete using bio-inspired neural network." Buildings 12 (2022a): 65, doi:10.3390/buildings12010065

Sun, J., Wang, Y., Li, K., Yao, X., Zhu, B., Wang, J., et al. 2022b, Molecular interfacial properties and engineering performance of conductive fillers in cementitious composites." *J. Mater. Res. Technol.* 19 (2022): 591–604. doi:10.1016/j.jmrt.2022.05.061

Sun, J., Wang, Y., Yao, X., Ren, Z., Zhang, G., Zhang, C., et al. Machine-learning-aided prediction of flexural strength and ASR expansion for waste glass cementitious composite." *Appl. Sci.* 11 (2021a): 6686, doi:10.3390/app11156686

Sun, Y., Li, G., Zhang, J., Sun, J., Huang, J., and Taherdangkoo, R. New insights of grouting in coal mass: from small-scale experiments to microstructures.*Sustainability*, 13, 2021b, 9315, doi:10.3390/su13169315

Szeląg, M., and Fic, S. *The use of image analysis techniques to describe a cluster cracks in the cement paste with the addition of metakaolinite.* 2016.

Thomas, J. J., and Jennings, H. M. A colloidal interpretation of chemical aging of the CSH gel and its effects on the properties of cement paste. *Cem. Concr. Res.*, 2006, 36(1): 30–38. doi:10.1016/j.cemconres.2004.10.022

Wang, B., Yan, L., Fu, Q., and Kasal, B. A comprehensive review on recycled aggregate and recycled aggregate concrete. *Resour. Conservation Recycl.*, 2021, 171: 105565, doi:10.1016/j.resconrec.2021.105565

Wang, Z., Gu, S., Chen, S., et al. Effect of fiber on mechanical properties and microstructure of ultra-high performance concrete. *J. Guangxi Univ. Sci. Technol.*,2023,34(01):20–27.

Wilhelm, S., and Kind, M. 2015 Influence of pH, temperature and sample size on natural and enforced syneresis of precipitated silica. *Polym. (Basel)* 7, 2504–2521. doi:10.3390/polym7121528

Wu, H., Guo, J., and Zhang, Yu. Orthogonal test on compressive strength of hybrid fiber reinforced concrete. *Sci. Technol. Eng.*,2022,22(32):14370–14378.

Xu, L., Huang, L., Chi, Y., and Mei, G. Tensile behavior of steel-polypropylene hybrid fiber-reinforced concrete.*Aci Mater. J.*, 2016, 113(2):219–229. doi:10.14359/51688641

Xuan, D. X., Shui, Z. H., and Wu, S. P. Influence of silica fume on the interfacial bond between aggregate and matrix in near-surface layer of concrete. *Constr. Build. Mater.*, 2009, 23(7): 2631–2635. doi:10.1016/j.conbuildmat.2009.01.006

Yan, B. *Experimental study on mechanical properties and frost resistance of modified coal gangue aggregate concrete.* Xi 'an, Xi 'an University of Architecture and Technology,2017a.

Yu, L., Xia, J., Xia, Z., Chen, M., Wang, J., and Zhang, Y. Study on the mechanical behavior and micro-mechanism of concrete with coal gangue fine and coarse aggregate. *Constr. Build. Mater.*, 2022, 338: 127626, doi:10.1016/j.conbuildmat.2022.127626

Zhang, G., Chen, C., Sun, J., Li, K., Xiao, F., Wang, Y., et al. 2022c, Mixture optimisation for cement-soil mixtures with embedded GFRP tendons." *J. Mater. Res. Technol.* 18 (2022): 611–628. doi:10.1016/j.jmrt.2022.02.076

Zhang, G., Wang, J., Jiang, Z., Peng, C., Sun, J., Wang, Y., et al. 2022a, Properties of sustainable self-compacting concrete containing activated jute fiber and waste mineral powders." *J. Mater. Res. Technol.* 19 (2022): 1740–1758. doi:10.1016/j.jmrt.2022.05.148

Zhang, N., Zhao, Z., and Zheng, C. Compression behavior of GFRP–coal gangue concrete–steel tubular columns. *Int. J. Press. Vessels Pi*, 2022b, 197: 104650, doi:10.1016/j.ijpvp.2022.104650

Zhang, S., Zheng, S., Wang, E., and Dai, H. Grey model study on strength and pore structure of self-compacting concrete with different aggregates based on NMR. *J. Build. Eng.*, 2023b, 64: 105560, doi:10.1016/j.jobe.2022.105560

Zhang, T., Wen, Q., Gao, S., and Tang, J. Comparative study on mechanical and environmental properties of coal gangue sand concrete. *Constr. Build. Mater.*, 2023a, 400: 132646, doi:10.1016/j.conbuildmat.2023.132646

Zhou, M., Dou, Y., Zhang, Y., and Zhang, B. Effects of the variety and content of coal gangue coarse aggregate on the mechanical properties of concrete. *Constr. Build. Mater.*,2019,220(30):386–395. doi:10.1016/j.conbuildmat.2019.05.176

Zhou, M., Wang, Q., and Mou, S. Study on effect of coarse aggregate characteristics of spontaneous combustion coal gangue on workability of concrete mix. *Non-metallic Mines*,2013,36(01):8–11.

Zhou, M., Tian, S., Guo, T., et al. Experimental study on preparation of concrete by spontaneous combustion of coal gangue. *Bull. Silic.*,2011,30(05):1221–1226.

Zhu, M., Qiu, J., and Chen, J. Effect and mechanism of coal gangue concrete modification by basalt fiber. *Constr. Build. Mater.*, 2022, 328: 126601, doi:10.1016/j.conbuildmat.2022.126601